Spectrum of sprite halos

F. J. Gordillo-Vázquez,[1] A. Luque,[1] and M. Simek[2]

Received 16 March 2011; revised 8 July 2011; accepted 9 August 2011; published 22 September 2011.

[1] Spectra of sprite halos in the spectral ranges 200–500 nm and 640–1065 nm are calculated for different spectral resolutions (between 2 nm and 10 nm), rotational temperatures (220 K and 1000 K) and observation altitudes corresponding to mountain (3 km and 4.3 km), airplane (14 km), balloon (35 km) and space observation platforms. We have calculated the non-equilibrium vibrational distribution functions (VDF) of different excited electronic states of molecular nitrogen (N_2) associated to sprite halo optical emissions in the ultraviolet (UV), due to the N_2 Lyman-Birge-Hopfield (LBH) and Vegard-Kaplan (VK) band systems, and near UV, visible and near infrared (NIR) due to the first (1PG) and second positive (2PG) bands of N_2. Comparison of synthetic sprite halo spectra with the single sprite halo spectrum existing to date shows reasonable agreement after the observed sprite halo spectra was corrected for instrument sensitivity response. Calculated VDFs of the $N_2(B^3\Pi_g)$ and $N_2(C^3\Pi_u)$ states of sprite halos show that the blue and NIR emissions produced through strong N_2-1PG ($B^3\Pi_g \rightarrow A^3\Sigma_u^+$) and N_2-2PG ($C^3\Pi_u \rightarrow B^3\Pi_g$) transitions are generally similar to those of known sprite spectral emission patterns, but differences may be observable at some vibrational levels. The calculated sprite halo spectra can be used as a predictive tool for the expected spectral emissions of sprite halos in different possible scenarios.

Citation: Gordillo-Vázquez, F. J., A. Luque, and M. Simek (2011), Spectrum of sprite halos, *J. Geophys. Res.*, *116*, A09319, doi:10.1029/2011JA016652.

1. Introduction

[2] Sprite halos are a type of upper-atmospheric Transient Luminous Events (TLE) that may or may not be followed by a sprite. Halos are brief (2–10 ms), diffuse glow regions of light with diameters of less than 100 km occurring at 70–85 km altitude [*Barrington-Leigh et al.*, 2001; *Wescott et al.*, 2001; *Miyasato et al.*, 2002, 2003]. According to *Moudry et al.* [2003], halos tend to fall into two distinct categories with respect to their spatial structure. Thus, optical emissions from halos can be structured or unstructured although unstructured emissions seem to be more common [*Moudry et al.*, 2003]. So far, no models predict structured halos while unstructured halo emissions have been modeled by *Barrington-Leigh et al.* [2001] as emissions due to quasi-electrostatic (QE) fields generated by positive cloud-to-ground (+CG) lightning. Halos have been observed mostly with 17 ms time resolution CCD cameras while three events recorded by a high-speed (1000–3000 frames per second) imaging system in 1997 were the first high-speed sprite halo images published [*Barrington-Leigh et al.*, 2001]. Most of sprites and halos are produced by +CG but recent results indicate that a large number of −CG lightning may also generate dim halos that are hardly detectable with conventional video imaging systems [*Williams et al.*, 2007]. In addition, in recent halo space observations by *Frey et al.* [2007] all recorded halos were created by −CG flashes occurring predominantly over the open ocean.

[3] While imaging of sprite halos dates back to the first images recorded in 1996 from the Wyoming Infrared Observatory [*Heavner*, 2000], the only spectral observations of a sprite halo available to date were fortuitously recorded June 22, 1995, as later recognized by *Wescott et al.* [2001], during a short campaign on Mt. Evans, Colorado, focused on the recording of one of the first spectral measurements of sprites [*Hampton et al.*, 1996]. According to *Wescott et al.* [2001], the halo whose spectrum was detected in 1995 preceded a group of sprites and the spectrograph recorded wide horizontal emissions (the spectrograph slit was parallel to the horizon in the spectroscopic studies of *Hampton et al.* [1996]), which were dim compared to the narrow emissions corresponding to the sprites that occurred later on. The recorded N_2 1PG halo spectrum covered the spectral range between 550 nm and 840 nm and was integrated during 17 ms; no sprite was observed to emit in the same video field [*Wescott et al.*, 2001]. The distance to the sprites (and sprite halos) was approximately 500 km from Mt. Evans Observatory, located at 4.3 km altitude [*Hampton et al.*, 1996]. Although the viewing conditions were clear, the observed halo spectrum presented low signal levels due to the very brief duration of the halo emissions compared to standard video rates. The observed halo spectrum was not corrected for instrument spectral response [*Wescott et al.*, 2001] and presented much higher noise levels in the data than the

[1] Instituto de Astrofísica de Andalucía, CSIC, Granada, Spain.
[2] Department of Pulse Plasma Systems, Institute of Plasma Physics, Academy of Sciences of the Czech Republic, Prague, Czech Republic.

0148-0227/11/2011JA016652

observed sprite spectra recorded by *Hampton et al.* [1996] in the same 1995 observation campaign from Mt. Evans. The noise in the observed halo spectrum was present in the entire spectral range (550–840 nm) but it was especially intense between 550 nm and 640 nm due to scattered anthropogenic light since these observations were made from Mt. Evans looking directly over Denver, Colorado [*Heavner*, 2000]. The spectral resolution used for recording the observed halo spectrum is not clear. However, *Hampton et al.* [1996] reported spectra of the red emission from the N_2 first positive system in the spectral range between 540 nm and 840 nm (the same shown in the observed halo spectrum) using spectral resolutions of 6 nm and 10 nm with the spectrograph slit parallel to the horizon.

[4] The available N_2 1PG sprite halo observations are similar to existing sprite spectral emissions in the 640–840 nm range explored by the works of *Mende et al.* [1995] and *Hampton et al.* [1996] and, more recently, by the sprite spectral observations at different altitudes of *Kanmae et al.* [2007] with improved spectral (3 nm) and temporal resolution (3 ms).

[5] Here we present calculations of sprite halo spectra in the UV, visible and NIR spectral ranges for different spectral resolutions (between 2 nm and 10 nm), gas temperatures 220 K and 1000 K) and an observational altitude corresponding to mountain (3 km and 4.3 km), airplane (14 km), balloon (35 km) and space observation platforms. The calculated LBH, VK, 2PG and 1PG halo spectra are based on vibrational distribution functions (VDFs) obtained from a non-equilibrium kinetic model of sprite halos [*Gordillo-Vázquez*, 2008; *Gordillo-Vázquez and Donkó*, 2009; *Gordillo-Vázquez*, 2010; *Luque and Gordillo-Vázquez*, 2011]. The analysis of the VDFs and synthetic halo spectra suggests that the calculated 640–840 nm N_2 1PG spectral features of halo emissions are in good agreement with those present in the only halo spectrum recorded to date which is also similar to the available (low (10 nm) spectral resolution) sprite spectra in the 640–840 nm spectral range [*Hampton et al.*, 1996]. However, our analysis also shows that sprite halo spectral emissions in the NIR should significantly deviate from the expected NIR emissions from sprites. In addition, some of the blue and near UV emissions of halos might differ from those associated with the 2PG from sprites. Our analysis draws conclusions and predictions that could be confirmed in future dedicated campaigns for spectral measurements of halo emissions from different observational platforms.

2. Model and Sprite Halo Spectra Calculations

2.1. Model

[6] In order to model the neutral and vibrational non-equilibrium kinetics of sprite halos, we have used the full atmospheric kinetic model described in detail by *Gordillo-Vázquez* [2008] and *Gordillo-Vázquez* [2010] in the context of sprites. This model solves the coupled Boltzmann transport equation (to derive the electron energy distribution function (EEDF)) with the rate equations associated to each of the different species considered (electrons, ions, atoms and molecules) and each of the electronically and vibrationally excited species. In this way, all the kinetics are self-consistent, although, in the present approach, the electrodynamics are not consistently solved with the plasma kinetics since the Poisson equation is not considered. In this regard, it has been assumed that the time-dependent reduced electric field (E/N, where N is the gas density at a given altitude), within the sprite halo glowing plasma is an external parametric function that is calculated off-line with a sprite halo model that considers halos as due to quasi-electrostatic fields from lightning as originally proposed by *Barrington-Leigh et al.* [2001]. In particular, we have used the density model described by *Luque and Ebert* [2009, 2010] to calculate the profile of the reduced electric field causing sprite halos at 80 km altitude. To generate this profile we assumed a +CG discharge with a charge moment change of 500 C km discharged within 1 ms. The resulting reduced electric field has the shape of a pulse that peaks at 1 ms with amplitude close to 150 Td and then decays in a few milliseconds. The Townsend is the conventional unit for reduced electric fields, 1 Td = 10^{-17} V cm^2.

[7] The full atmospheric model of non-equilibrium kinetics of sprite halos includes now a number of changes. The old quenching rates used by *Gordillo-Vázquez* [2010], are replaced by new rates from *Piper* [1988] for quenching of $N_2(B^3\Pi_g)$ by N_2, *Morrill and Benesch* [1996] for quenching of $N_2(B^3\Pi_g)$ by O_2, *Dilecce et al.* [2006] for quenching of $N_2(C^3\Pi_u)$ by N_2 and from *Pancheshnyi* [2000] for quenching of $N_2(C^3\Pi_u)$ by O_2 [*Luque and Gordillo-Vázquez*, 2011]. In addition to the vibrational kinetics of $N_2(X^1\Sigma_g^+)$ and to that of the N_2 triplet states ($A^3\Sigma_u^+$, $B^3\Pi_g$, $C^3\Pi_u$, $W^3\Delta_u$, and $B'^3\Sigma_u^+$) already considered by *Gordillo-Vázquez* [2010] and *Broadfoot et al.* [1997], we have now also included the vibrational kinetics of the N_2 singlet state $a^1\Pi_g$ with vibrational levels from v = 0 to v = 15. We assume that the production of $N_2(a^1\Pi_g)$ is mainly driven by collisions of electrons with $N_2(X^1\Sigma_g^+,\ \nu = 0)$, with integral cross sections taken from *Cartwright et al.* [1977]. In order to extract the absolute cross sections for the electron-impact excitation of each of the considered vibrational levels of $N_2(a^1\Pi_g)$ due to collisions with $N_2(X^1\Sigma_g^+, \nu = 0)$, we have used the procedure described by *Borst and Chang* [1973].

[8] On the other hand, we disregard the radiative decay between $N_2(w^1\Delta_u)$ and $N_2(a^1\Pi_g)$ but consider the radiative cascading between $N_2(a^1\Pi_g, \nu = 0-15)$ and $N_2(a'^1\Sigma_u^-, \nu = 0)$, although it might not persist long enough to radiate due to predissociation. The kinetic scheme of $N_2(a'^1\Sigma_u^-, \nu = 0)$ is the same already used by *Gordillo-Vázquez* [2008]. In addition, since both $a^1\Pi_g$ and $B^3\Pi_g$ states have the same electronic configuration and differ only in their spin coupling, it is then reasonable that the v-dependent quenching rates of $N_2(a^1\Pi_g)$ by N_2 proceeds at the same rate as the one of $N_2(B^3\Pi_g)$ by N_2 [*Cartwright*, 1978]. It is also assumed here that the v-dependent quenching rates of $N_2(a^1\Pi_g)$ by O_2 are one order of magnitude faster than quenching by N_2 [*Eastes*, 2000]. Thus, the v-dependent quenching rates of $N_2(a^1\Pi_g)$ by N_2 and O_2 used here are the ones given by *Piper* [1988, 1992], respectively. We have considered the LBH band system by including the set of radiative transitions between $N_2(a^1\Pi_g, \nu = 0-6)$ ($N_2(a^1\Pi_g, \nu > 6)$ predissociates before radiating) and $N_2(X^1\Sigma_g^+, \nu = 0-21)$ with radiative transition rates taken from *Gilmore et al.* [1992]. Finally, we have also considered that $N_2(a^1\Pi_g, \nu = 0)$ can be lost due to the collisional processes $N_2(a^1\Pi_g, \nu = 0) + N_2(a^1\Pi_g, \nu = 0) \rightarrow N_2 + N_2^+ + e$

and $N_2(a^1\Pi_g, \nu = 0) + O_2 \rightarrow N_2 + 2O$ with rates given by *Starikovskaia et al.* [2001] and $N_2(a^1\Pi_g, \nu = 0) + NO \rightarrow N_2 + N + O$, with rate coefficients from *Kossyi et al.* [1992].

[9] According to *Eastes and Dentamaro* [1996] the collisional-induced electronic transitions (CIET) observed in laboratory measurements may significantly influence emissions from the LBH bands. Therefore, the CIET could contribute, in addition to radiative decay, to the loss of the lower vibrational levels the $N_2(a^1\Pi_g)$ and $N_2(a'^1\Sigma_u^-)$ [*Eastes*, 2000]. Measurements by *Eastes and Dentamaro* [1996] suggest that, in auroras, radiative transitions between N_2 singlet states are less important than CIET. However, present theoretical understanding of CIET is incomplete [*Eastes*, 2000] and only CIET rates based only on extrapolations from similar transitions are available with the consequent large uncertainties [*Eastes and Dentamaro*, 1996]. Therefore, we have not included CIET for the kinetics of $N_2(a^1\Pi_g)$ and $N_2(a'^1\Sigma_u^-)$ in sprite halos considered here. However, we have included similar results obtained by *Morrill and Benesch* [1996] in connection with the electronic triplet states of N_2 which overlapping vibrational level concentrations are importantly affected by processes of intersystem collisional transfer of excitation (ICT). The ICT processes controlling $N_2(B^3\Pi_g)$ and the other N_2 triplets are incorporated in the present sprite halo model using the rates proposed by *Morrill and Benesch* [1996].

[10] Out of the 14 loss processes considered (5 collisional) for $N_2(a^1\Pi_g, \nu = 0)$, electronic quenching by O_2 is the most important closely followed by some LBH radiative decay transitions toward $N_2(X^1\Sigma_g^+, \nu = 2)$, $N_2(X^1\Sigma_g^+, \nu = 3)$ and $N_2(X^1\Sigma_g^+, \nu = 1)$. After these four, electronic quenching by N_2 is the most important. The other three collisional de-excitation processes of $N_2(a^1\Pi_g, \nu = 0)$ are of much less importance than $N_2(a^1\Pi_g, \nu = 0)$ LBH radiative decays.

[11] The kinetic model considered for the sprite halo emissions also includes the basic mechanisms controlling the production and loss of the first negative (1NG) band of N_2^+ and of the Rydberg ($A^2\Sigma^+$, $C^2\Pi_r$) and valence ($B^2\Pi$) electronic states of nitride oxide (NO). The generation of N_2^+ ($B^2\Sigma_u^+$) is possible through direct electron-impact excitation from $N_2(X^1\Sigma_u^+)$ [*Borst and Zipf*, 1970] and N_2^+ ($X^2\Sigma_g^+$) [*Orel et al.*, 1990]. The loss of $N_2^+(B^3\Sigma_u^+)$ is controlled by collisional mechanisms such as quenching by N_2 and O_2 [*Dilecce et al.*, 2010] and associative ion conversion $N_2^+(B^3\Sigma_u^+) + N_2 + M \rightarrow N_4^+ + M$ [*Pancheshnyi*, 2006], and by radiative decays $N_2^+(B^3\Sigma_u^+) \rightarrow N_2^+(X^2\Sigma_g^+) + h\nu$ with radiative rates taken from *Gilmore et al.* [1992].

[12] For the electronic states of NO considered, electron-impact excitation of $NO(A^2\Sigma^+)$, $NO(C^2\Pi_r)$ and $NO(B^2\Pi)$ have been incorporated to the kinetic model using the electron-impact cross sections updated by *Brunger et al.* [2000] and *Liu and Pasko* [2010]. We assumed that $NO(A^2\Sigma^+)$ can also be produced by $N_2(A^3\Sigma_u^+, \nu = 0) + NO(X^2\Pi_r) \rightarrow NO(A^2\Sigma^+) + N_2(X^1\Sigma_g^+, \nu = 0)$ and by the three-body processes $N + O + N_2 \rightarrow NO(A^2\Sigma^+) + N_2$ and $N + O + O_2 \rightarrow NO(A^2\Sigma^+) + O_2$, with rates given by *Simek* [2003] and *Capitelli et al.* [2000] (for the three-body mechanisms), respectively. The loss of $NO(A^2\Sigma^+)$ is assumed to be due to the collisional mechanisms $NO(A^2\Sigma^+) + O_2 \rightarrow NO(X^2\Pi_r) + O_2$ [*Simek*, 2003] and $NO(A^2\Sigma^+) + N_2(X^1\Sigma_g^+, \nu = 0) \rightarrow NO(X^2\Pi_r) + N_2(A^3\Sigma_u^+, \nu = 0)$ [*Thoman et al.*, 1992] and to radiative transitions such as the $NO - \gamma$ emission ($\simeq$227 nm), $NO(A^2\Sigma^+) \rightarrow NO(X^2\Pi_r) + h\nu$ [*Cleary et al.*, 1995]. The kinetics of $NO(C^2\Pi_r)$ and $NO(B^2\Pi)$ are driven by electron-impact excitation from $NO(X^2\Pi_r)$ and by the three-body processes $N + O + N_2 \rightarrow NO(B^2\Pi, C^2\Pi_r) + N_2$ and $N + O + O_2 \rightarrow NO(B^2\Pi, C^2\Pi_r) + O_2$ [*Capitelli et al.*, 2000]. On the other hand, the loss of $NO(C^2\Pi_r)$ and $NO(B^2\Pi)$ is assumed to be mainly due to $NO - \delta$ emission ($\simeq$191 nm), $NO(C^2\Pi_r) \rightarrow NO(X^2\Pi_r) + h\nu$, and $NO - \beta$ emission ($\simeq$220 nm), $NO(B^2\Pi) \rightarrow NO(X^2\Pi_r) + h\nu$.

2.2. Sprite Halo Spectra Calculations

[13] Spectrometric representation of various electronically excited species can be done by calculating synthetic emission spectra. The full atmospheric kinetic model used in this work emphasizes the importance of N_2 ($a^1\Pi_g$, $A^3\Sigma_u^+$, $B^3\Pi_g$ and $C^3\Pi_u$) state populations for predicting optical emissions that might be produced and detected under sprite halo conditions. The N_2 triplet states are responsible for the 2PG and 1PG emissions through the $C^3\Pi_u \rightarrow B^3\Pi_g \rightarrow A^3\Sigma_u^+$ radiative cascade covering nearly all UV-vis-NIR spectral range, while the $a^1\Pi_g \rightarrow X^1\Sigma_g^+$ singlet transition gives rise to the Lyman-Birge-Hopfield (LBH) system occurring mainly in the VUV.

[14] To model emission of the 1PG, 2PG and LBH systems, we applied an approach based on calculating all allowed transitions between rotational manifolds of the upper and lower vibronic states arranged in a sequence of bands [*Simek et al.*, 1995; *Simek*, 2002]. In this work, we considered all allowed rotational transitions between $N_2(C^3\Pi_u, \nu = 0 - 4)$, $N_2(B^3\Pi_g, \nu = 0 - 12)$, $N_2(A^3\Sigma_u^+, \nu = 0 - 20)$, $N_2(a^1\Pi_g, \nu = 0 - 15)$ and $N_2(X^1\Sigma_g^+, \nu = 0 - 21)$ states with the intensity of a single rotational line given by

$$I_j(T_R) = const \times n_j(T_R) \frac{\nu_j^4 \varphi_j}{2J_j + 1}, \quad (1)$$

where ν_j, φ_j, J_j and n_j are, respectively, the frequency, the Hönl-London factor, the rotational quantum number ($\leq$40) and the population of the corresponding upper state level, each for the j-th rotational line; T_R stands for the rotational temperature given by Boltzmann rotational population of emitting levels [*Whiting et al.*, 1980; *Herzberg*, 1950]. Regarding the 1PG and 2PG emissions, we used an approach described in detail by *Simek et al.* [1995] and *Simek* [2002] which was developed to generate synthetic spectra of 1PG and 2PG systems, respectively. To achieve the highest precision, the frequencies ν_j were calculated by diagonalizing Hamiltonians with matrix elements and equilibrium molecular constants derived from high-resolution experiments by *Roux et al.* [1983, 1989, 1993]. Concerning the LBH system, we employed molecular constants provided by *Trickl et al.* [1995]. After creating band profiles for all bands of a given system, we composed the complete spectrum of the LBH/1PG/2PG system for the vibrational distributions obtained by the kinetic modeling using the Einstein coefficients given by *Gilmore et al.* [1992]. All bands were modeled assuming the Boltzmann rotational temperatures of $T_R = 220$ K and 1000 K and convolved with triangular line-shapes corresponding to resolutions ranging from $\Delta\lambda = 0.14$ nm to $\Delta\lambda = 10$ nm.

[15] The spectral resolution is the key issue when evaluating vibrational distributions and/or rotational temperatures from partially resolved roto-vibronic structure of emission

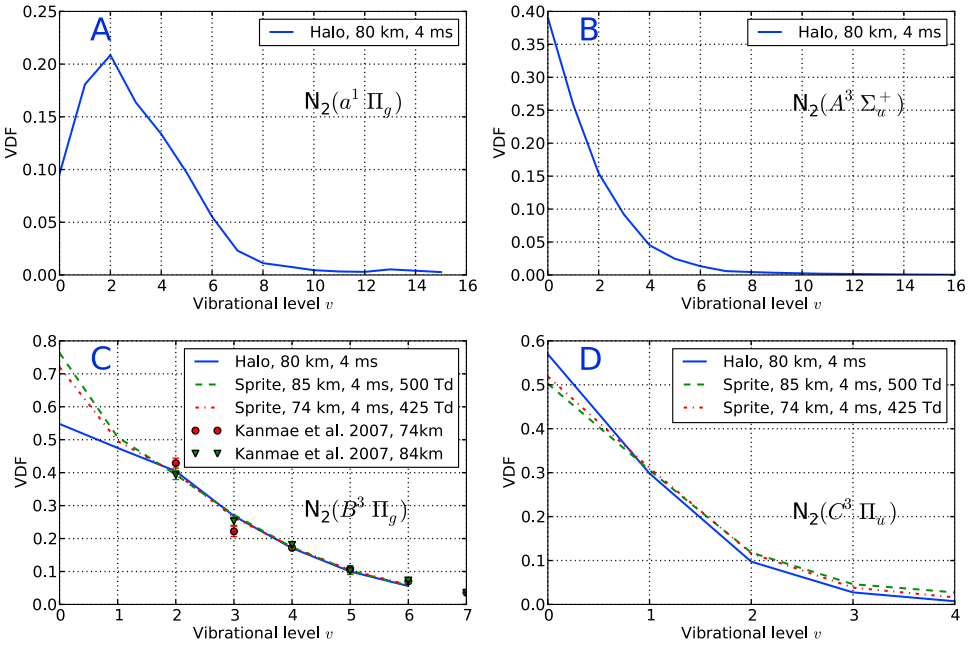

Figure 1. Calculated VDF for (a) $N_2(a^1\Pi_g)$, (b) $N_2(A^3\Sigma_u^+)$, (c) $N_2(B^3\Pi_g)$ and (d) $N_2(C^3\Pi_u)$ for sprite halos occurring at 80 km using a temporal resolution of 4 ms. For comparison, Figure 1c shows the sprite $N_2(B^3\Pi_g)$ VDF at 74 km and 85 km as calculated by *Luque and Gordillo-Vázquez* [2011] and observed by *Kanmae et al.* [2007] with 3 ms temporal resolution. Figure 1d compares the calculated VDF of $N_2(C^3\Pi_u)$ for sprite halos at 80 km (present work, solid line) and sprites at 74 km and 85 km (dashed lines) [*Luque and Gordillo-Vázquez*, 2011]. The normalization of the VDFs is described in the text.

bands of diatomics. The T_R = 1000 K was selected here somewhat arbitrarily in order to demonstrate limits of low resolution spectra to provide vibrational/rotational temperatures. We have produced synthetic spectra for various spectral resolution $\Delta\lambda$ (0.14 nm and 2–10 nm).

[16] Even when resolving obstacles caused by the atmospheric transmittance, the VUV singlet spectra of the LBH can hardly be used to reveal vibrational distributions with some structures (such as shown in Figure 1a) or evaluate rotational temperatures for resolutions $\Delta\lambda \geq 2$ nm (typically used for experimental observations) due to a significant overlapping of several vibrational sequences in the 120–220 nm spectral range. To evaluate the vibrational distribution from the LBH emission correctly, spectral resolution $\Delta\lambda < 1$ nm would be required.

[17] In the case of the 2PG N_2 system, spectral resolution $\Delta\lambda \approx 2$ nm seems to be quite sufficient to evaluate correctly vibrational distributions (and to reveal, for example, differences between the VDF in halos and the VDF in sprites as shown in Figure 1d) using $\Delta\nu = -2, -3, -4$ sequences and to estimate or verify rotational temperature from the unresolved rotational structure of the (0,1), (0,2) or (0,3) bands which may offer a reasonable compromise between the transition probabilities of the bands, efficiency of the detection system and signal attenuation due to the atmospheric transmittance.

[18] The best conditions to evaluate rotational temperatures are evidently given by the 1PG N_2 system. Due to small spin splitting, the 1PG N_2 bands are composed of three sub-bands whose relative intensities are temperature dependent [*Simek and DeBenedictis*, 1995]. Partially resolved rotational structures of e.g. (3,0), (2,0) or (1,0) bands obtained using $\Delta\lambda \gtrsim$ 2 nm resolution instrument would then allow quite confident T_R evaluation.

3. Results and Discussion

[19] The calculated VDFs for $N_2(a^1\Pi_g)$, $N_2(A^3\Sigma_u^+)$ $N_2(B^3\Pi_g)$ and $N_2(C^3\Pi_u)$ are shown in Figures 1a, 1b, 1c, and 1d, respectively. All VDFs correspond to sprite halos at 80 km altitude and optical emissions integrated during 4 ms. For comparison we have also represented the calculated VDFs associated to the 1PG (Figure 1c) and 2PG (Figure 1d) N_2 band emissions from sprites at 74 km and 85 km altitudes [*Luque and Gordillo-Vázquez*, 2011] together with the VDF derived from 1PG observed sprites (Figure 1c) at the same altitudes [*Kanmae et al.*, 2007]. The VDFs represent population densities of vibrational levels relative to the total density of the electronic state; i.e. they are normalized such that the sum of the values of each vibrational state equals one. The exception is the VDF of $N_2(B^3\Pi_g)$, where only states with ν = 2 to 6 are included in the normalization in order to compare with available observations (see below).

[20] The VDF of $N_2(a^1\Pi_g)$ associated to the LBH emissions from a sprite halo at 80 km is shown in Figure 1a. Unfortunately there are no observations of such LBH VDF from halos nor sprites so a comparison with TLE observational data is not possible. However, the calculated $N_2(a^1\Pi_g)$ VDF of halos shown in Figure 1a exhibits qualitative agreement with the relative vibrational populations of the $N_2(a^1\Pi_g)$ as derived from the N_2 LBH band emission observations in the Earth's dayglow reported by *Budzien et al.* [1994] including the peaking around ν = 2 to ν = 3. The LBH emission in the Earth's dayglow reported by *Budzien et al.* [1994] become

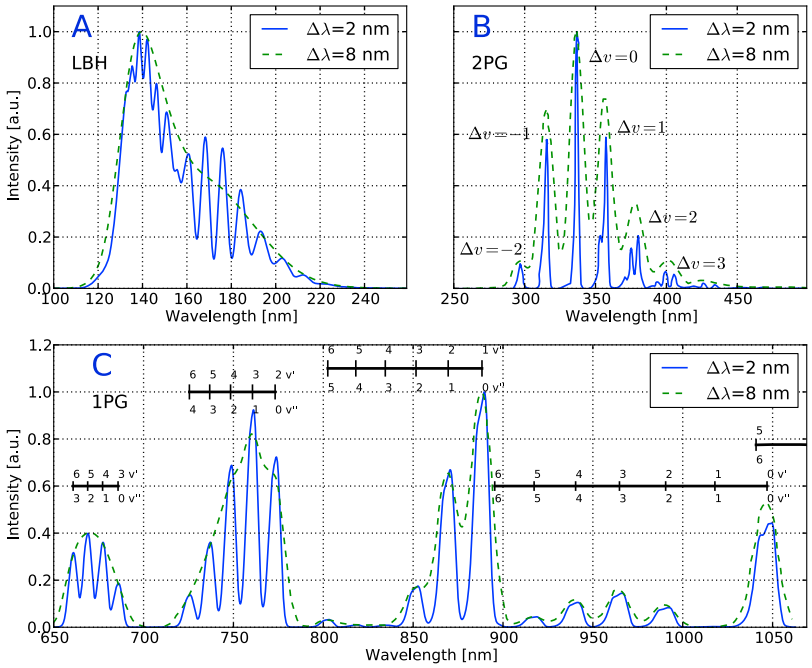

Figure 2. Calculated spectra (uncorrected by atmospheric transmittance) for sprite halo optical emissions of the (a) LBH, (b) 2PG and (c) 1PG of N_2 in the 100–260 nm, 250–500 nm and 650–1065 nm spectral ranges, respectively. All the spectra have been calculated for a rotational temperature of T_R = 220 K and two spectral resolutions $\Delta\lambda$ = 2 nm (solid line) and $\Delta\lambda$ = 8 nm (dashed line). The spectra are normalized with respect to the LBH(2,0), 2PG(0,0) and 1PG(1,0) transitions at 138.4 nm, 337.0 nm and 888.3 nm, respectively.

unreliable for ν = 6 due to systematic errors in the data analysis [*Eastes*, 2000].

[21] Figure 1b shows the calculated VDF of $N_2(A^3\Sigma_u^+)$ corresponding to the forbidden Vegard-Kaplan (VK) band emissions in the ultraviolet. The VK band emissions are not detectable during sprite halo emissions because $N_2(A^3\Sigma_u^+)$ is a metastable electronic state with optical emissions taking place in a timescale much longer than the duration of halos, thus allowing the quenching of $N_2(A^3\Sigma_u^+, \nu)$ by N_2, O_2 and O that collisionally deactivate $N_2(A^3\Sigma_u^+, \nu)$ preventing VK emissions. In addition, we have also considered the lost of $N_2(A^3\Sigma_u^+)$ due to collisions with oxygen atoms producing NO [*Campbell et al.*, 2007]. The quenching rates of $N_2(A^3\Sigma_u^+)$ by N_2, O_2 and O have a gas temperature dependence as $T^{1/2}$ (with T in Kelvin) [*Sentman et al.*, 2008]. This can cause a slight difference of less than 20% between quenching rates of $N_2(A^3\Sigma_u^+)$ by N_2, O_2 and O at sea level ($T \approx$ 300 K) and in the mesosphere ($T \approx$ 200 K).

[22] As can be seen in Figure 1c, both halo and sprite 1PG N_2 VDFs are quite similar from ν = 2 through ν = 6, which explains the similarity detected between sprite and halo spectral features in the visible (640–840 nm) region of the 1PG N_2 band emissions [*Wescott et al.*, 2001]. A difference is seen in the ν = 0 level, where the halo vibrational population is approximately 20–30% lower than that of sprites.

[23] Finally, Figure 1d shows that according to our normalization, the sprite and halo vibrational distributions of the $N_2(C^3\Pi_u)$ state differ from each other by ~10% in the ν = 0,2 vibrational levels. The consequence is that 2PG progressions involving the ν = 0,1 and 2 levels of the $N_2(C^3\Pi_u)$ state will produce slightly different patterns in the near UV and blue regions of sprite and halo spectra.

[24] Emission spectra for the LBH, 2PG and 1PG of N_2 without correction for atmospheric transmittance are shown in Figures 2a, 2b, and 2c, respectively. The comparison presented in each plot corresponds to calculated sprite halo spectra at 80 km altitude assuming a rotational temperature (T_R) of 220 K and two spectral resolutions ($\Delta\lambda$) of 2 nm and 8 nm. The fine structure associated with the higher spectral resolution (2 nm) is clearly visible when compared to the lower spectral resolution case (8 nm). In addition, the strong 1PG N_2 NIR emissions in the 850–900 nm spectral range and beyond 1000 nm are shown in Figure 2c.

[25] Figure 3 shows calculated spectra for sprite halo optical emissions of the 2PG of N_2 in the 250–500 nm spectral range for T_R = 220 K and $\Delta\lambda$ = 2 nm (Figure 3a), T_R = 1000 K and $\Delta\lambda$ = 2 nm (Figure 3b), T_R = 220 K and $\Delta\lambda$ = 8 nm (Figure 3c) and T_R = 1000 K and $\Delta\lambda$ = 8 nm (Figure 3d). The plots have been corrected for atmospheric transmittance using MODTRAN predictions [*Anderson et al.*, 1993]. The transmittances were calculated assuming a 500 km atmospheric path length from mountain (3 km and 4.3 km), airplane (14 km) and balloon (35 km) platforms, respectively, pointing to sprite halos at 80 km altitude. For space observations, we assume an observer at 400 km altitude looking at the nadir and limb corrected for atmospheric transmittance through, respectively, 320 km and 2000 km atmospheric path lengths neglecting absorption above 100 km altitude. The calculated band spectra of molecular nitrogen were multiplied by the atmospheric transmittance and convolved with a triangular

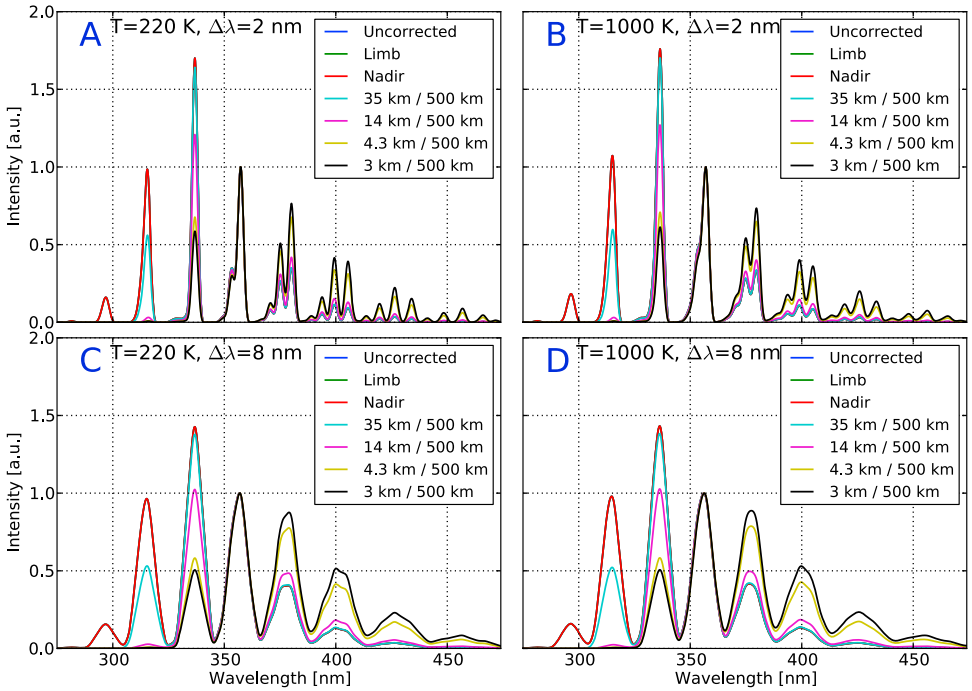

Figure 3. Calculated spectra for sprite halo optical emissions of the 2PG of N_2 in the 250–500 nm spectral range for (a) $T_R = 220$ K and $\Delta\lambda = 8$ nm, (b) $T_R = 1000$ K and $\Delta\lambda = 8$ nm, (c) $T_R = 220$ K and $\Delta\lambda = 2$ nm and (d) $T_R = 1000$ K and $\Delta\lambda = 2$ nm. The plots have been corrected for atmospheric transmittance assuming a 500 km atmospheric path length from mountains (3 km and 4.3 km), airplane (14 km) and balloon (35 km) pointing to sprite halos at 80 km altitude. For space observations, we assume an observer at 400 km altitude looking at the nadir and limb corrected for atmospheric transmittance through, respectively, 320 km and 2000 km atmospheric path lengths neglecting absorption above 100 km. The spectra are normalized with respect to the (0,1) transition at 357.6 nm. Note that the uncorrected, limb and nadir spectra are superimposed.

slit function, of different full width at half maximum (FWHM), to produce the synthetic spectra at different spectral resolutions. As spectral resolution improves (at the same rotational temperature) finer spectral structure becomes apparent. On the other hand, the impact of increasing the rotational temperature (at fixed spectral resolution) is to smooth spectral features as can be seen by comparing Figures 3a and 3b for $\Delta\lambda = 2$ nm at 357.6 nm, 370.9 nm and 380.4 nm. We can conclude from Figure 3 that, although the 2PG N_2 emissions could be detected from high altitude (14 km) airplanes, the best locations to observe NUV and blue spectral emissions from halos would be space platforms and stratospheric balloons [*Heavner et al.*, 2010], since only these observations would reveal the sub-bands with the shortest wavelengths.

[26] Halo optical emissions associated to the 1PG of N_2 are shown in Figure 4 in the 650–1065 nm spectral range for $T_R = 220$ K and $\Delta\lambda = 2$ nm (Figure 4a), $T_R = 1000$ K and $\Delta\lambda = 2$ nm (Figure 4b), $T_R = 220$ K and $\Delta\lambda = 8$ nm (Figure 4c) and $T_R = 1000$ K and $\Delta\lambda = 8$ nm (Figure 4d). The plots have been corrected for atmospheric transmittance following the procedure mentioned above. The spectra in Figures 4a–4d are normalized to the (2,1) transition at 773.2 nm and it appears clear that the visible and NIR emissions from the 1PG of N_2 excited in sprite halos could be recorded from both low and high altitude observation platforms although more efficient detection in the 650–800 nm could be obtained from airplanes, stratospheric balloons and space. The $\Delta\nu = 1$ and 0 sequences of the 1 PG emissions (850–1060) could be, in principle, recorded from high mountains.

[27] The calculated LBH emission spectrum from sprite halos occurring behind the limb, in the limb and in the nadir of an observing satellite are shown in Figure 5 for different spectral resolutions ($\Delta\lambda$ = 0.14 nm, 2 nm and 8 nm) and corrected for atmospheric transmittance. We calculated the transmittance resulting from these three observation geometries:

[28] 1. Behind-the-limb simulating observations from the Imager of Sprites and Upper Atmospheric Lightnings (ISUAL) aboard the FORMOSAT-2 satellite. The observer is located at 900 km altitude and looks at the halo through a path of 4300 km. We used the transmittance from *Kuo et al.* [2007, Figure 7] (tangent height 80 km).

[29] 2. In the limb, simulating an observation from an instrument at the International Space Station (ISS), orbiting at about 400 km altitude, looking at the limb and observing a halo at 80 km through an optical path of 2000 km.

[30] 3. In the nadir, where an observer at the ISS observes a halo directly 320 km below.

[31] The limb and nadir transmittances are calculated from the absorption cross sections of *Minschwaner et al.* [1992] for

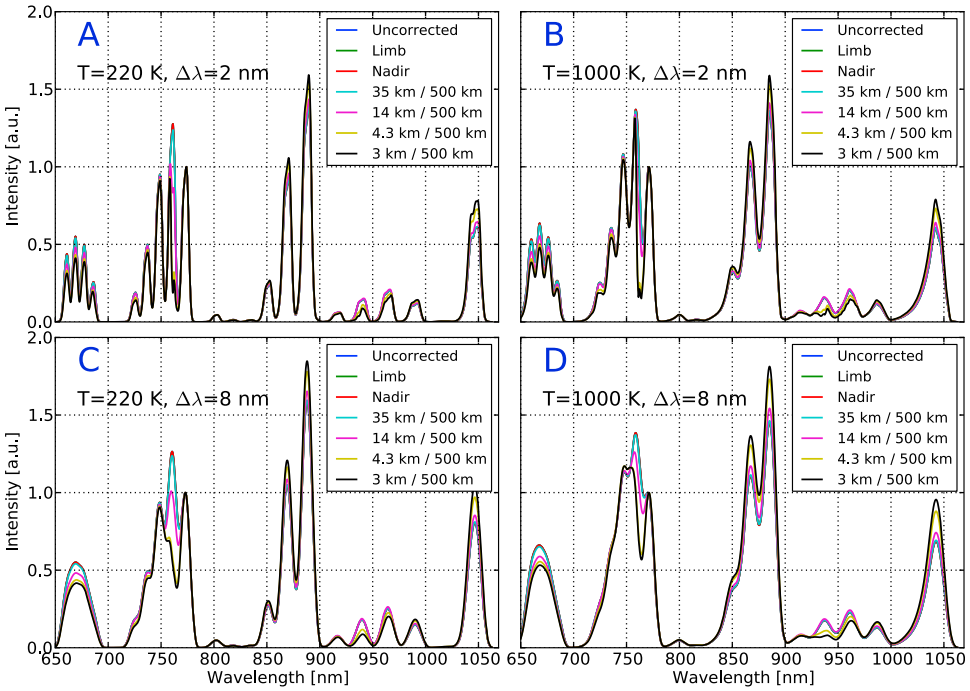

Figure 4. Calculated spectra for sprite halo optical emissions of the 1PG of N_2 in the 650–1065 nm spectral range for (a) $T_R = 220$ K and $\Delta\lambda = 8$ nm, (b) $T_R = 1000$ K and $\Delta\lambda = 8$ nm, (c) $T_R = 220$ K and $\Delta\lambda = 2$ nm and (d) $T_R = 1000$ K and $\Delta\lambda = 2$ nm. The plots have been corrected for atmospheric transmittance assuming a 500 km atmospheric path length from mountains (3 km and 4.3 km), airplane (14 km) and balloon (35 km) pointing to sprite halos at 80 km altitude. For space observations, we assume an observer at 400 km altitude looking at the nadir and limb corrected for atmospheric transmittance through, respectively, 320 km and 2000 km atmospheric path lengths neglecting absorption above 100 km. The spectra are normalized with respect to the (2,0) transition at 773.2 nm. Note that the uncorrected, limb and nadir spectra are superimposed.

the Schumann-Runge band of O_2 (using a gas temperature of 200 K), *Cheung et al.* [1986] for the Herzberg continuum of O_2 (measured at 295 K) and *Molina and Molina* [1986] for the ozone absorption. The numerical values were obtained from H. Keller-Rudek and K. K. Moortgat (MPI-Mainz-UV-VIS spectral atlas of gaseous molecules, available at www.atmosphere.mpg.de/spectral-atlas-mainz).

[32] Comparison of Figure 5 to Figure 2a shows that halo LBH spectral emissions could be better recorded from space by looking at the nadir, rather than limb or behind-limb events. Far UV (FUV) emissions from halos have been detected by ISUAL from space [*Frey et al.*, 2007; *Kuo et al.*, 2008; *Chang et al.*, 2010]. However, due to the short (≤0.1 ms) delay time between the parent lightning and the halo emission, ISUAL can only process the detection of FUV emission from halos occurring behind the limb [*Kuo et al.*, 2008]. For the ISUAL observation, the before and behind the limb events are 2800 km and 4300 km away, respectively, from the satellite due to the geometry imposed by the high altitude (almost 900 km) of ISUAL. For halos occurring behind the limb, the halo FUV emissions suffer substantial atmospheric attenuation and, consequently, the chance to detect significant halo FUV signal is considerably reduced. The detection of halo FUV could be improved by observations from lower orbit instruments such as the Atmospheric Space Interaction Monitor (ASIM) nadir photometer (145–230 nm bandpass and 61.4° × 61.4° FOV) that will be placed on the external platform of the Columbus module of the ISS located between 340 km and 400 km altitude. Depending on resolution, Figure 5 shows the expected sensitivity to LBH UV emission in the nadir could be a factor of two higher at 190 nm and an order of magnitude higher at 180 nm than the corresponding sensitivities in the limb observations.

[33] Finally, we have represented in Figure 6 the synthetic spectra for sprite halo optical emissions of the 1PG of N_2 in the 650–1065 nm spectral range for $\Delta\lambda = 10$ nm (Figure 6a), $\Delta\lambda = 9$ nm (Figure 6b), $\Delta\lambda = 6$ nm (Figure 6c) and $\Delta\lambda = 2$ nm (Figure 6d). All plots have been calculated for $T_R = 220$ K and 1000 K and corrected for atmospheric transmittance assuming a 500 km atmospheric path length from a mountain platform at 4.3 km altitude (like Mt. Evans in Colorado, USA) pointing to sprite halos at 80 km altitude. The only available sprite halo spectra (with some features of the 1PG N_2 emission), serendipitously recorded by *Hampton et al.* [1996] in June 22, 1995 and later on published in 2001 [*Wescott et al.*, 2001], has been included for comparison in Figures 6a and 6b after correcting for instrument sensitivity response in the 640–820 nm spectral range. The spectra are normalized with respect to the (2,1) transition at 773.2 nm and we show the original data (red solid line) and the case where we have removed noise by uniformly reducing the signal level by 15% relative to the (2,1) peak (red dashed line). Noise sources

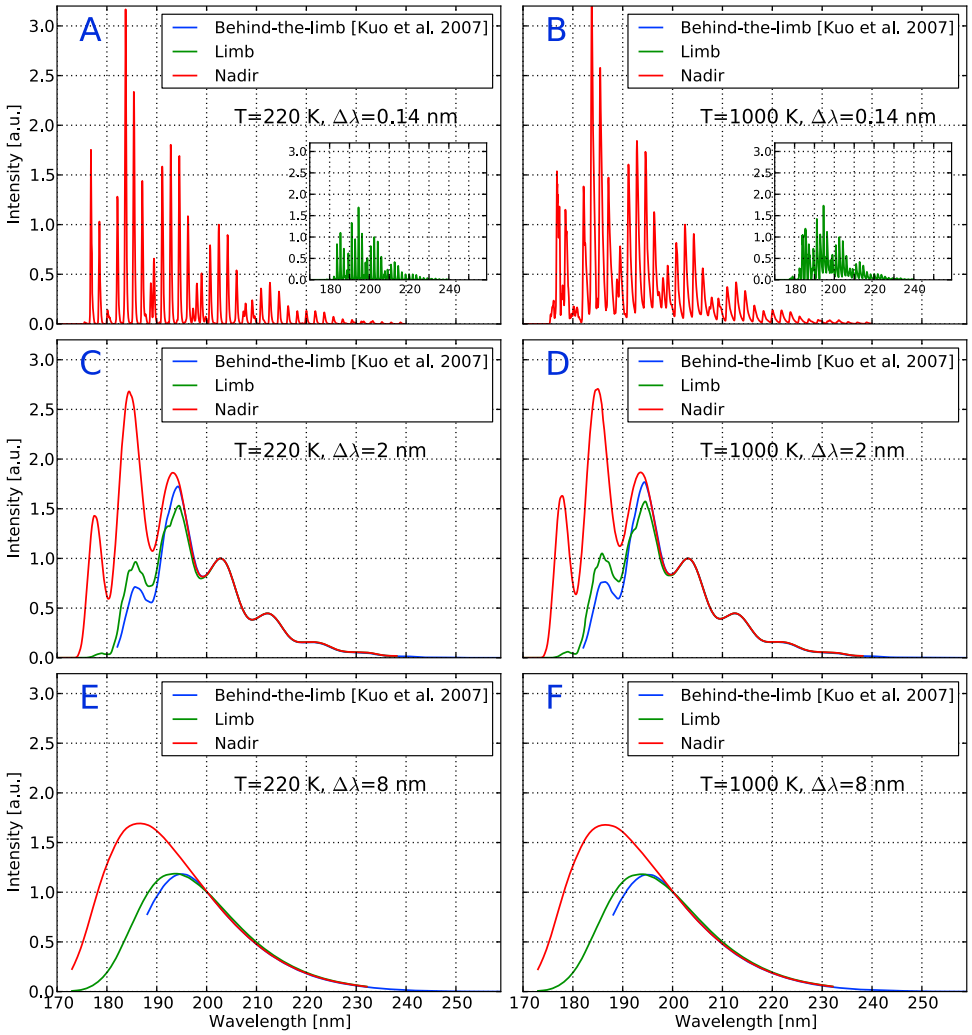

Figure 5. Calculated spectra for sprite halo optical emissions of the LBH of N_2 in the 170–260 nm spectral range for (a) $T_R = 220$ K and $\Delta\lambda = 0.14$ nm, (b) $T_R = 1000$ K and $\Delta\lambda = 0.14$ nm, (c) $T_R = 220$ K and $\Delta\lambda = 2$ nm, (d) $T_R = 1000$ K and $\Delta\lambda = 2$ nm, (e) $T_R = 220$ K and $\Delta\lambda = 8$ nm and (f) $T_R = 1000$ K and $\Delta\lambda = 8$ nm. The behind-the-limb plots in Figures 5c–5f have been corrected for atmospheric transmittance assuming observation from a satellite about 4300 km away from a sprite halo at 80 km altitude. The transmittance in this case is taken from Figure 7 of *Kuo et al.* [2007] which do not have enough resolution for extracting data at 0.14 nm spectral resolution. The insets in Figures 5a and 5b have the same scale and normalization that the plots corresponding to the nadir. The spectra are normalized with respect to the (3,11) transition at 200.7 nm.

include anthropogenic light as well as thermal and electronic instrumental noise associated with low signal intensity and short integration times of 17 ms [*Wescott et al.*, 2001]. The value of 15% is provided as an example of a plausible level of noise that would improve significantly the match between the observation and our model.

[34] The agreement between the observed halo spectra and the present spectra model predictions is quite reasonable. The comparison between the calculated and the observed halo spectra suggests that the observed one was recorded with a spectral resolution of 9 nm or 10 nm and that the background rotational temperature was close to 220 K. In addition, we note that while the 762 nm emission corresponding to the 1PG N_2 (3,1) is visible in the 6 nm and 3 nm spectral resolution sprite spectra by *Hampton et al.* [1996] and *Kanmae et al.* [2007], respectively, it was almost not visible in the 10 nm spectral resolution sprite spectrum reported by *Hampton et al.* [1996] and, interestingly, it was completely absent in the observed halo spectrum recorded in 22 June, 1995 during the 1995 sprite spectroscopy campaign from Mt. Evans, Colorado [*Hampton et al.*, 1996]. We think that the absence of the 762 emission in the observed halo spectrum is an indication of the low spectral resolution (probably around 10 nm) set in the moment of the halo spectrum recording.

[35] The first 1PG N_2 NIR spectroscopic studies (up to 900 nm) from sprites emissions at 53–57 km altitude were made back in 1996 from the Wyoming Infrared Observatory

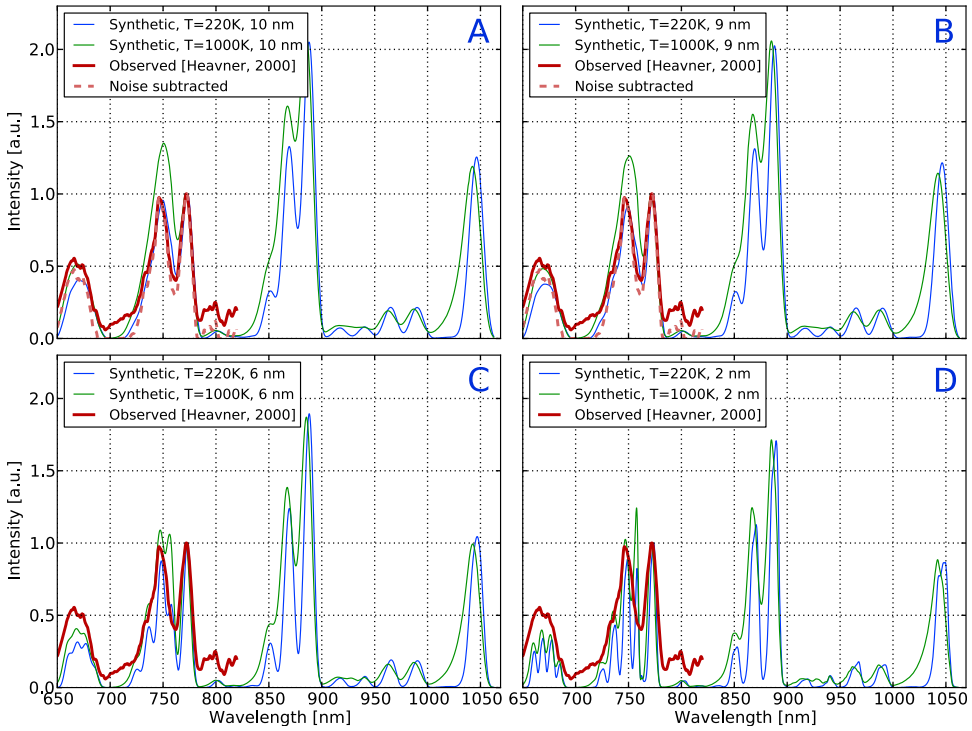

Figure 6. Calculated spectra for sprite halo optical emissions of the 1PG of N_2 in the 650–1065 nm spectral range for (a) $\Delta\lambda = 10$ nm, (b) $\Delta\lambda = 9$ nm, (c) $\Delta\lambda = 6$ nm and (d) $\Delta\lambda = 2$ nm. All plots have been calculated for $T_R = 220$ K and 1000 K and corrected for atmospheric transmittance assuming a 500 km atmospheric path length from a mountain platform at 4.3 km altitude (like Mt. Evans in Colorado, USA) pointing to sprite halos at 80 km altitude. The only available sprite halo spectra (with some features of the 1PG N_2 emission), serendipitously recorded by *Hampton et al.* [1996] in June 22, 1995 and later on published in 2001 [*Wescott et al.*, 2001], has been included for comparison in Figures 6a and 6b after correcting for instrument sensitivity response in the 640–820 nm spectral range and considering the original noise (red solid line) and the case with 15% uniform noise substraction (red dashed line). The spectra are normalized with respect to the (2,1) transition at 773.2 nm.

(WIRO) on Jelm Mountain (at 3 km altitude) [*Morrill et al.*, 1998; *Bucsela et al.*, 2003]. Since then, the only sprite NIR imaging campaign took place during the EXL98 airborne (13.5 km altitude) observing mission with a low pixel resolution (128 × 128) camera [*Siefring et al.*, 2010] where the first images of NIR (900–1700 nm) sprite emissions were taken but no recording was performed of the 1PG N_2 spectroscopic emissions in the 900–1700 nm spectral range. It is important to note that the red 1PG N_2 emissions are the brightest in sprites [*Mende et al.*, 1995; *Hampton et al.*, 1996; *Morrill et al.*, 1998; *Bucsela et al.*, 2003; *Kanmae et al.*, 2007] and that much of the 1PG N_2 $\Delta\nu < 2$ emissions are in the NIR spectral range [*Siefring et al.*, 2010]. Therefore, since most of our present understanding of the energetics of TLEs (particularly of sprites, halos and elves) comes from analysis and interpretation of optical data in the visible, we think, following *Siefring et al.* [2010], that dedicated NIR spectroscopic campaigns are needed to carefully track the 1PG N_2 bands with the highest optical (brightness) energy in the 800–1700 nm range.

[36] Our analysis has shown that the 1PG N_2 VDF of halos and sprites are almost equal for vibrational levels above $\nu = 2$ but differ for $\nu = 0$ and $\nu = 1$. Consequently, halo and sprite spectra are expected to be almost the same in the visible (550–800 nm) though their NIR emission patterns are predicted to be different. In addition, we have also found that 2PG N_2 VDFs of halo and sprites are slightly different and this could influence their NUV and blue optical emissions in a way that both halos and sprites could also exhibit distinct NUV and blue spectral features.

4. Summary and Conclusions

[37] We have calculated spectra of sprite halos in the 200–500 nm and 640–1065 nm spectral ranges using spectral resolutions between 2 nm and 10 nm, rotational temperatures of 220 K and 1000 K and considering observation platforms located in mountains (3 km and 4.3 km), airplane (14 km), balloon (35 km) and space. Using a full atmospheric kinetic model for sprites and halos, we have been able to calculate the non-equilibrium VDFs of the electronic states of N_2 involved in sprite halo optical emissions in the UV, particularly for the LBH and VK band systems, and the near UV, visible and NIR due to the 2PG and 1PG, respectively. The comparison of the synthetic sprite halo spectra with the only sprite halo spectrum recorded so far shows a reasonable agreement after correcting the sprite halo spectra for instrument sensitivity response. On the other hand, the calculated VDFs of the $N_2(B^3\Pi_g)$ and $N_2(C^3\Pi_u)$ states in sprite halos indicate that the blue and NIR emissions (especially those involving $\nu' = 0$)

produced through strong N_2 2PG and N_2 1PG transitions can differ from the known sprite spectral emission patterns. Apart from the visible sprite halo spectrum available between 640 nm and 820 nm, no UV, NIR or IR sprite halo spectra have been measured to date. The present results suggest that NIR emissions (especially those involving $\nu' = 0$) from sprite halos can differ (above error uncertainties) from those of sprites and, therefore, present calculations can be used as a predictive tool for expected spectral emissions of sprite halos as measured from several observation platforms in different scenarios.

[38] **Acknowledgments.** We thank T. Kanmae for kindly providing instrument spectral response curves of the Deehr spectrograph in the 640–820 nm spectral range. This work was supported by the Spanish Ministry of Science and Innovation, MICINN under project AYA2009-14027-C05-02 and by the Junta de Andalucia, Proyecto de Excelencia FQM-5965.

[39] Robert Lysak thanks the reviewers for their assistance in evaluating this paper.

References

Anderson, G. P., et al. (1993), MODTRAN2: Suitability for remote sensing, in *Atmospheric Propagation and Remote Sensing*, vol. 2, edited by A. Kohnle and W. B. Miller, *Proc. SPIE*, *1968*, 514.

Barrington-Leigh, C. P., U. S. Inan, and M. Stanley (2001), Identification of sprites and elves with intensified video and broadband array photometry, *J. Geophys. Res.*, *106*, 1741, doi:10.1029/2000JA000073.

Borst, W. L., and S. L. Chang (1973), Excitation of metastable $N_2(A^3\Sigma_u^+)$ vibrational levels by electron impact, *J. Chem. Phys.*, *59*, 5830, doi:10.1063/1.1679950.

Borst, W. L., and E. C. Zipf (1970), Cross section for electron-impact excitation of the (0,0) first negative band of N_2^+ from threshold to 3 keV, *Phys. Rev. A*, *1*, 834, doi:10.1103/PhysRevA.1.834.

Broadfoot, A. L., D. B. Hatfield, E. R. Anderson, T. C. Stone, B. R. Sandel, J. A. Gardner, E. Murad, D. J. Knecht, C. P. Pike, and R. A. Viereck (1997), N_2 triplet band systems and atomic oxygen in the dayglow, *J. Geophys. Res.*, *102*, 11,567, doi:10.1029/97JA00771.

Brunger, M. J., L. Campbell, D. C. Cartwright, A. G. Middleton, B. Mojarrabi, and P. J. O. Teubner (2000), Electron-impact excitation of Rydberg and valence electronic states of nitric oxide: II. Integral cross sections, *J. Phys. B At. Mol. Phys.*, *33*, 809, doi:10.1088/0953-4075/33/4/315.

Bucsela, E., J. Morrill, M. Heavner, C. Siefring, S. Berg, D. Hampton, D. Moudry, E. Wescott, and D. Sentman (2003), $N_2(B^3\Pi_g)$ and $N_2^+(A^2\Pi_u)$ vibrational distributions observed in sprites, *J. Atmos. Sol. Terr. Phys.*, *65*, 583, doi:10.1016/S1364-6826(02)00316-4.

Budzien, S. A., P. D. Feldman, and R. R. Conway (1994), Observations of the far ultraviolet airglow by the Ultraviolet Limb Imaging experiment on STS-39, *J. Geophys. Res.*, *99*, 23,275, doi:10.1029/94JA01543.

Campbell, L., D. C. Cartwright, and M. J. Brunger (2007), Role of excited N_2 in the production of nitric oxide, *J. Geophys. Res.*, *112*, A08303, doi:10.1029/2007JA012337.

Capitelli, M., C. M. Ferreira, B. F. Gordiets, and A. I. Osipov (2000), *Plasma Kinetics in Atmospheric Gases*, Springer, Berlin.

Cartwright, D. C. (1978), Vibrational populations of the excited states of N_2 under auroral conditions, *J. Geophys. Res.*, *83*, 517, doi:10.1029/JA083iA02p00517.

Cartwright, D. C., S. Trajmar, A. Chutjian, and W. Williams (1977), Electron impact excitation of the electronic states of N_2. II. Integral cross sections at incident energies from 10 to 50 eV, *Phys. Rev. A*, *16*, 1041, doi:10.1103/PhysRevA.16.1041.

Chang, S. C., et al. (2010), Far-ultraviolet events, elves, and lightning current, *J. Geophys. Res.*, *115*, A00E46, doi:10.1029/2009JA014861.

Cheung, A. S.-C., K. Yoshino, W. H. Parkinson, D. E. Freeman, and S. L. Guberman (1986), Absorption cross section measurements of oxygen in the wavelength region 195–241 nm of the Herzberg continuum, *Planet. Space Sci.*, *34*, 1007, doi:10.1016/0032-0633(86)90011-5.

Cleary, D. D., S. Gnanalingam, R. P. McCoy, K. F. Dymond, and F. G. Eparvier (1995), The middle ultraviolet dayglow spectrum, *J. Geophys. Res.*, *100*, 9729, doi:10.1029/94JA03145.

Dilecce, G., P. F. Ambrico, and S. De Benedictis (2006), OODR-LIF direct measurement of $N_2(C^3\ \Pi u, v = 0–4)$ electronic quenching and vibrational relaxation rate coefficients by N_2 collision, *Chem. Phys. Lett.*, *431*, 241, doi:10.1016/j.cplett.2006.09.094.

Dilecce, G., P. F. Ambrico, and S. De Benedictis (2010), On the collision quenching of N_2^+ ($B^2\Sigma_u^+$, v = 0) by N_2 and O_2 and its influence on the measurement of E/N by intensity ratio of nitrogen spectral bands, *J. Phys. D*, *43*(19), 195201, doi:10.1088/0022-3727/43/19/195201.

Eastes, R. W. (2000), Modeling the N_2 Lyman-Birge-Hopfield bands in the dayglow: Including radiative and collisional cascading between the singlet states, *J. Geophys. Res.*, *105*, 18,557, doi:10.1029/1999JA000378.

Eastes, R. W., and A. V. Dentamaro (1996), Collision-induced transitions between the $a^1\Pi_g$, $a'^1\Sigma_u^-$, and $w^1\Delta_u$ states of N_2: Can they affect auroral N_2 Lyman-Birge-Hopfield band emissions?, *J. Geophys. Res.*, *101*, 26,931, doi:10.1029/96JA01636.

Frey, H. U., et al. (2007), Halos generated by negative cloud-to-ground lightning, *Geophys. Res. Lett.*, *34*, L18801, doi:10.1029/2007GL030908.

Gilmore, F. R., R. R. Laher, and P. J. Espy (1992), Franck-Condon factors, r-centroids, electronic transition moments, and Einstein coefficients for many nitrogen and oxygen band systems, *J. Phys. Chem. Ref. Data*, *21*, 1005, doi:10.1063/1.555910.

Gordillo-Vázquez, F. J. (2008), Air plasma kinetics under the influence of sprites, *J. Phys. D*, *41*, 234016, doi:10.1088/0022-3727/41/23/234016.

Gordillo-Vázquez, F. J. (2010), Vibrational kinetics of air plasmas induced by sprites, *J. Geophys. Res.*, *115*, A00E25, doi:10.1029/2009JA014688.

Gordillo-Vázquez, F. J., and Z. Donkó (2009), Electron energy distribution functions and transport coefficients relevant for air plasmas in the troposphere: Impact of humidity and gas temperature, *Plasma Sources Sci. Technol.*, *18*, 034021, doi:10.1088/0963-0252/18/3/034021.

Hampton, D. L., M. J. Heavner, E. M. Wescott, and D. D. Sentman (1996), Optical spectral characteristics of sprites, *Geophys. Res. Lett.*, *23*, 89, doi:10.1029/95GL03587.

Heavner, M. J. (2000), Optical spectroscopic observations of sprites, blue jets, and elves: Inferred microphysical processes and their macrophysical implications, Ph.D. thesis, Univ. of Alaska Fairbanks, Fairbanks.

Heavner, M. J., J. S. Morrill, C. Siefring, D. D. Sentman, D. R. Moudry, E. M. Wescott, and E. J. Bucsela (2010), Near-ultraviolet and blue spectral observations of sprites in the 320–460 nm region: N_2 (2PG) emissions, *J. Geophys. Res.*, *115*, A00E44, doi:10.1029/2009JA014858.

Herzberg, G. (1950), *Molecular Spectra and Molecular Structure I. Spectra of Diatomic Molecules*, Van Nostrand Reinhold, New York.

Kanmae, T., H. C. Stenbaek-Nielsen, and M. G. McHarg (2007), Altitude resolved sprite spectra with 3 ms temporal resolution, *Geophys. Res. Lett.*, *34*, L07810, doi:10.1029/2006GL028608.

Kossyi, I. A., A. Y. Kostinsky, A. A. Matveyev, and V. P. Silakov (1992), Kinetic scheme of the non-equilibrium discharge in nitrogen-oxygen mixtures, *Plasma Sources Sci. Technol.*, *1*, 207, doi:10.1088/0963-0252/1/3/011.

Kuo, C.-L., et al. (2007), Modeling elves observed by FORMOSAT-2 satellite, *J. Geophys. Res.*, *112*, A11312, doi:10.1029/2007JA012407.

Kuo, C. L., et al. (2008), Radiative emission and energy deposition in transient luminous events, *J. Phys. D*, *41*, 234014, doi:10.1088/0022-3727/41/23/234014.

Liu, N., and V. P. Pasko (2010), NO-γ emissions from streamer discharges: Direct electron impact excitation versus resonant energy transfer, *J. Phys. D*, *43*, 082001, doi:10.1088/0022-3727/43/8/082001.

Luque, A., and U. Ebert (2009), Emergence of sprite streamers from screening-ionization waves in the lower ionosphere, *Nat. Geosci.*, *2*, 757, doi:10.1038/ngeo662.

Luque, A., and U. Ebert (2010), Sprites in varying air density: Charge conservation, glowing negative trails and changing velocity, *Geophys. Res. Lett.*, *37*, L06806, doi:10.1029/2009GL041982.

Luque, A., and F. J. Gordillo-Vázquez (2011), Modeling and analysis of $N_2(B^3\Pi_g)$ and $N_2(C^3\Pi_u)$ vibrational distributions in sprites, *J. Geophys. Res.*, *116*, A02306, doi:10.1029/2010JA015952.

Mende, S. B., R. L. Rairden, G. R. Swenson, and W. A. Lyons (1995), Sprite spectra: N_2 1 PG band identification, *Geophys. Res. Lett.*, *22*, 2633, doi:10.1029/95GL02827.

Minschwaner, K., G. P. Anderson, L. A. Hall, and K. Yoshino (1992), Polynomial coefficients for calculating O_2 Schumann-Runge cross sections at 0.5/cm resolution, *J. Geophys. Res.*, *97*, 10,103.

Miyasato, R., M. J. Taylor, H. Fukunishi, and H. C. Stenbaek-Nielsen (2002), Statistical characteristics of sprite halo events using coincident photometric and imaging data, *Geophys. Res. Lett.*, *29*(21), 2033, doi:10.1029/2001GL014480.

Miyasato, R., H. Fukunishi, Y. Takahashi, and M. J. Taylor (2003), Energy estimation of electrons producing sprite halos using array photometer data, *J. Atmos. Sol. Terr. Phys.*, *65*, 573, doi:10.1016/S1364-6826(02)00322-X.

Molina, L. T., and M. J. Molina (1986), Absolute absorption cross sections of ozone in the 185- to 350-nm wavelength range, *J. Geophys. Res.*, *91*, 14,501, doi:10.1029/JD091iD13p14501.

Morrill, J. S., and W. M. Benesch (1996), Auroral N_2 emissions and the effect of collisional processes on N_2 triplet state vibrational populations, *J. Geophys. Res.*, *101*, 261, doi:10.1029/95JA02835.

Morrill, J. S., E. J. Bucsela, V. P. Pasko, S. L. Berg, M. J. Heavner, D. R. Moudry, W. M. Benesch, E. M. Wescott, and D. D. Sentman (1998), Time resolved N_2 triplet state vibrational populations and emissions associated with red sprites, *J. Atmos. Sol. Terr. Phys.*, *60*, 811, doi:10.1016/S1364-6826(98)00031-5.

Moudry, D., H. Stenbaek-Nielsen, D. Sentman, and E. Wescott (2003), Imaging of elves, halos and sprite initiation at 1ms time resolution, *J. Atmos. Sol. Terr. Phys.*, *65*, 509, doi:10.1016/S1364-6826(02)00323-1.

Orel, A. E., T. N. Rescigno, and B. H. Lengsfield III (1990), Theoretical study of electron-impact excitation of N_2^+, *Phys. Rev. A*, *42*, 5292, doi:10.1103/PhysRevA.42.5292.

Pancheshnyi, S. (2000), Collisional deactivation of $N_2(C^3\Pi_u,\nu = 0, 1, 2, 3)$ states by N_2, O_2, H_2 and H_2O molecules, *Chem. Phys.*, *262*, 349, doi:10.1016/S0301-0104(00)00338-4.

Pancheshnyi, S. (2006), Comments on 'Intensity ratio of spectral bands of nitrogen as a measure of electric field strength in plasmas,' *J. Phys. D*, *39*, 1708, doi:10.1088/0022-3727/39/8/N01.

Piper, L. G. (1988), State-to-state $N_2(A\ ^3\Sigma_u^+)$ energy pooling reactions. II. The formation and quenching of $N_2(B^3\Pi_g, v = 1–12)$, *J. Chem. Phys.*, *88*, 6911, doi:10.1063/1.454388.

Piper, L. G. (1992), Energy transfer studies on $N_2(X^1\Sigma_g^+,v)$ and $N_2(B^3\Pi_g)$, *J. Chem. Phys.*, *97*, 270, doi:10.1063/1.463625.

Roux, F., F. Michaud, and J. Verges (1983), High-resolution Fourier spectrometry of $^{14}N_2$ infrared emission spectrum: Extensive analysis of the $B^3\Pi_g - A^3\Sigma_u^+$ system, *J. Mol. Spectrosc.*, *97*, 253, doi:10.1016/0022-2852(83)90266-7.

Roux, F., F. Michaud, and M. Vervloet (1989), High-resolution Fourier spectrometry of $^{14}N_2$: Analysis of the (0-0), (0-1), (0-2), (0-3) bands of the $C^3\Pi_u - B^3\Pi_g$ system, *Can. J. Phys.*, *67*, 143.

Roux, F., F. Michaud, and M. Vervloet (1993), High-resolution Fourier spectrometry of $^{14}N_2$ violet emission spectrum: Extensive analysis of the $C^3\Pi_u \rightarrow B^3\Pi_g$ system, *J. Mol. Spectrosc.*, *158*, 270, doi:10.1006/jmsp.1993.1071.

Sentman, D. D., H. C. Stenbaek-Nielsen, M. G. McHarg, and J. S. Morrill (2008), Plasma chemistry of sprite streamers, *J. Geophys. Res.*, *113*, D11112, doi:10.1029/2007JD008941.

Siefring, C. L., J. S. Morrill, D. D. Sentman, and M. J. Heavner (2010), Simultaneous near-infrared and visible observations of sprites and acoustic-gravity waves during the EXL98 campaign, *J. Geophys. Res.*, *115*, A00E57, doi:10.1029/2009JA014862.

Simek, M. (2002), The modelling of streamer-induced emission in atmospheric pressure, pulsed positive corona discharge: N_2 second positive and NO-γ systems, *J. Phys. D*, *35*, 1967, doi:10.1088/0022-3727/35/16/311.

Simek, M. (2003), Determination of $N_2(A\ ^3\Sigma_u^+)$ metastable density produced by nitrogen streamers at atmospheric pressure: 1. Design of diagnostic method, *Plasma Sources Sci. Technol.*, *12*, 421, doi:10.1088/0963-0252/12/3/318.

Simek, M., and S. DeBenedictis (1995), On the use of the numerical simulation of the first positive system of N_2: 2. Fast T_{rot} estimation from the partially resolved (3,0) band, *Plasma Chem. Plasma Process.*, *15*, 451–463.

Simek, M., G. Dilecce, and S. DeBenedictis (1995), On the use of the numerical simulation of the first positive system of N_2: 1. Emission and LIF analysis, *Plasma Chem. Plasma Process.*, *15*, 427–449.

Starikovskaia, S. M., A. Y. Starikovskii, and D. V. Zatsepin (2001), Hydrogen oxidation in a stoichiometric hydrogen-air mixture in the fast ionization wave, *Combust. Theory Modell.*, *5*, 97.

Thoman, J. W., Jr., J. A. Gray, J. L. Durant Jr., and P. H. Paul (1992), Collisional electronic quenching of $NO(A^2\Sigma^+)$ by N_2 from 300 to 4500 K, *J. Chem. Phys.*, *97*, 8156, doi:10.1063/1.463437.

Trickl, T., D. Proch, and K. L. Kompa (1995), The Lyman-Birge-Hopfield system of nitrogen: Revised calculation of the energy levels, *J. Mol. Spectrosc.*, *171*(2), 374–384, doi:10.1006/jmsp.1995.1126.

Wescott, E. M., H. C. Stenbaek-Nielsen, D. D. Sentman, M. J. Heavner, D. R. Moudry, and F. T. S. Sabbas (2001), Triangulation of sprites, associated halos and their possible relation to causative lightning and micrometeors, *J. Geophys. Res.*, *106*, 10,467, doi:10.1029/2000JA000182.

Whiting, E. E., A. Schadee, J. B. Tatum, J. T. Hougen, and R. W. Nicholls (1980), Recommended conventions for defining transition moments and intensity factors in diatomic molecular spectra, *J. Mol. Spectrosc.*, *80*, 249, doi:10.1016/0022-2852(80)90137-X.

Williams, E., E. Downes, R. Boldi, W. Lyons, and S. Heckman (2007), Polarity asymmetry of sprite-producing lightning: A paradox?, *Radio Sci.*, *42*, RS2S17, doi:10.1029/2006RS003488.

F. J. Gordillo-Vázquez and A. Luque, Instituto de Astrofísica de Andalucía, CSIC, PO Box 3004, E-18080 Granada, Spain. (vazquez@iaa.es; aluque@iaa.es)

M. Simek, Department of Pulse Plasma Systems, Institute of Plasma Physics, Academy of Sciences of the Czech Republic, Za Slovankou 3, 182 00 Prague, Czech Republic. (simek@ipp.cas.cz)